sustainability

MDPI

Article

The Flow Law of Brine and Sediment Particles in Gas-Driven Brine Drainage in the Sediments of Salt Cavern Gas Storage

Yi Zhang [1,*], Jun Lu [2], Jun Li [1], Yan Liu [1] and Erdong Yao [3]

[1] PetroChina Research Institute of Petroleum Exploration and Development, Beijing 100083, China; lij69@petrochina.com.cn (J.L.); liuyan1968@petrochina.com.cn (Y.L.)
[2] Science and Technology Information Center of West-East Gas Transmission Co., Ltd., Shanghai 200122, China; lujun@pipechina.com.cn
[3] State Key Laboratory of Petroleum Resources and Prospecting, China University of Petroleum, Beijing 102249, China; yaoed@cup.edu.cn
* Correspondence: zhangyi15@petrochina.com.cn

Abstract: The geological resources of salt cavern gas storage in China are mostly complex layered salt beds with many thin inter-layers and high insoluble matter content. In the process of cavity-building by water-solution method, the insoluble matters in salt layers and inter-layers are peeled off and deposited at the bottom of salt cavern, occupying more than one-third of the whole cavity volume. These sediments have a large pore volume and strong compressibility, and they are filled with brine; as a result, they have great potential for gas storage. The research on the flow law of brine and sediment particles in gas-driven brine drainage in the sediments of salt caverns is the basis of utilizing the void space of sediments for gas storage. In this paper, salt cores of salt cavern gas storage wells in the Jintan District were selected, and the physical characteristics of insoluble sediments of the salt cores were analyzed. Then, a laboratory simulation device and experimental method of the gas-driven brine drainage were presented. Using artificial composite sediments in the experimental device, the following was tested: (i) the flow rates of brine and particles in the vicinity of the brine drain pipe in the sediments under different nitrogen displacement pressures, (ii) the relationship between the sand extraction amount and nitrogen displacement pressure of different brine drain pipes, (iii) the sand extraction amount of different sizes of particles with brine drain time, (iv) the cumulative sand extraction amount of different brine drain pipes, and (v) the effect of brine flow rate on the sand extraction amount. The results show that quartz, plagioclase, and ankerite account for 45–94% and clay accounts for 3.3–14.4% of the insoluble minerals of the salt cores from the Jintan District. The particle size distribution of the sediments ranges from 0.04 mm to 6 mm and can be divided into four ranges: <0.5 mm, 0.5 mm~2 mm, 2 mm~4 mm, and >4 mm. The mass percentage of each range is 37.9%, 36.5%, 17%, and 8.6%, respectively. There is a threshold pressure of the gas-driven brine drainage, where the larger the diameter of the sieve hole, the lower the threshold pressure, and the easier the pipe is to sand out. The diameter of the sieve hole has a great influence on the flow rate of the sediment particles near the brine drain pipe. The increase in nitrogen displacement pressure has a positive correlation with the flow rate of sediments near the pipe with 5 mm diameter sieve holes, but has little effect on the flow rate of sediments near pipes with 1.5 mm or 0.5 mm diameter sieve holes. The sand extraction amount is affected by factors such as the nitrogen displacement pressure, diameter of sieve hole, brine drain time, and brine flow rate in the process of gas-driven brine drainage. A higher nitrogen displacement pressure and brine flow rate lead to more sand extraction. A screen pipe with 1 mm diameter sieve holes is suggested to be used for sand control, the sieve holes are recommended to be machined in the shape of a trumpet with a small inlet section (i.e., 1 mm) and a large outlet end (i.e., 1.5 mm), and the brine flow rate is suggested to be about 30 m^3/h when the brine removal is carried out in the sediments of salt cavern, which depends on the actual operation on site.

Keywords: salt cavern gas storage; insoluble sediment; physical properties; brine drain; flow law

Citation: Zhang, Y.; Lu, J.; Li, J.; Liu, Y.; Yao, E. The Flow Law of Brine and Sediment Particles in Gas-Driven Brine Drainage in the Sediments of Salt Cavern Gas Storage. *Sustainability* **2023**, *15*, 12613. https://doi.org/10.3390/su151612613

Academic Editor: Reza Daneshazarian

Received: 16 June 2023
Revised: 27 July 2023
Accepted: 10 August 2023
Published: 21 August 2023

1. Introduction

Salt caverns are becoming more and more prevalent in energy storage with their many advantages such as large storage capacity, high working gas ratio, large daily gas recovery, flexible market response, and good economy [1–3]. The first salt cavern was utilized in the early 1940s in Canada for storing liquefied petroleum gas. At present, there are 108 salt cavern gas storages in service all around the world [4,5]. Most cavities are constructed in a thick salt dome, located in Europe and America. However, the salt beds used to build salt caverns for gas storage in China generally contain many inter-layers such as mudstone or anhydrite, and the content of insoluble matters in the salt layer and inter-layer is relatively high [2,6,7]. The proportion of inter-layers in salt rocks ranges from 10% to 50%, the content of insoluble matters in salt bed is 5–40%, and the content of insoluble matter in inter-layer increases to 54–96% in the Jintan District, Ping-dingshan, Huai′an, and other regions [7–10].

Many scholars have carried out experimental tests and analyses on the dissolution characteristics of salt rocks with inter-layers and the collapse mechanism of the inter-layers. Liu et al. studied the dissolution characteristics of salt rock when the salt rock grade is 50% and 75% [11]. Zeng et al. tested the effect of the volume fraction of sodium chloride in brine on the dissolution rate of salt rocks with salt cores, Glauber′s salt ore, and Long Hills salt rock samples [12]. Zhang et al. developed a similar material for the geomechanical model of salt cavern gas storage, and simulated the salt rock, mudstone and inter-bed separately [13]. Zheng et al. proposed a new design method of fully soaking the inter-layer and building the trench one more time to enlarge the space for thick-sandwich salt cavern gas storage [14]. Zheng et al. tested the solubility, uni-axial and tri-axial compression of salt samples from the Huai′an, Ping-dingshan, and An-ning regions, and discovered that increasing confining pressure can restrain the influence of insoluble matter content on short-term strength of rock salt [15]. Liu et al. analyzed the influence of the permeability of three typical inter-layers on the tightness of energy storage in deep-bedded salt formations. The results showed that there was a low permeability in the compressed inter-layer, which was beneficial to the sealing performance of gas storage [16]. Ban et al. analyzed the rock salt grades influences on salt cavity gas storage built with water solution, and considered that salt cavity gas storage should be built in strata with high-grade-rock salts, which can not only control the configuration of the cavity, but also shorten the construction period [17]. Wang et al. combined field data and investigated the technology for controlling the collapse of a thick inter-layer during salt cavern construction [18]. All the above efforts have promoted the successful construction of salt cavern gas storages in multi-layered salt formations in China.

The complexity of the stratigraphic structure of salt beds has a great influence on the dissolution rate of salt water, the control of the cavity shape, the construction period of gas storage, and the storage volume of the salt cavern [19–22]. According to the statistics, the volume of insoluble sediments account for 33–66.2% of the total volume of salt cavern in such areas as Huai′An, Chouzhou, Pingdingshan, Yunying, and Jintan District, and the pores of the sediment are filled with brine [2–6]. It is the most common approach to inject gas into the salt cavity to drain brine [21–24]. In the field implementation, there is usually still 3~10 m depth of residual brine above the sediment surface after the completion of the operation of gas-driven brine drainage. This is mainly due to the vibration and bending deformation of brine drain pipes, as well as for safety operations. As a result, almost half the volume of the salt cavern is occupied by sediments and brine [3–7,21–24] (Figure 1).

The sediments at the bottom of the salt cavern are in a loose accumulation state with a high porosity, and they are filled with brine. In recent years, a large number of studies have been carried out on the physical properties of the sediments. Chen et al. carried out an experimental study on the dilatancy and expansion coefficient of sediment in multi-layered salt cavern gas storage, and analyzed the effects of shape, size, arrangement, and size distribution of the particles on the dilatancy coefficient of the inter-layers [25]. Ban et al. studied the influence of the content of insoluble matter in salt rock on the effective space of gas storage cavity [17]. Ren et al. used the gas expansion method to test the pore volume of sediments and concluded that the total porosity of the sediments at the bottom of a

salt cavern in Jintan District was 45.73%, while it was 42.66% measured by field sonar according to the pore volume model and calculation method [26]. On the basis of the experimental tests, Zhang et al. concluded that the volume of the sediment at the bottom of the cavity was nearly twice larger than it was before fragmentation and expansion, while the porosity was between 44% and 69% at atmospheric pressure. There was an exponential negative correlation between the sediment porosity and the overlying loading pressure [27]. Han et al. carried on an experiment and simulation to determine the void ratio of the sediment accumulation body. By combining laboratory physical experiment simulation with mathematical modeling, they obtained that the porosity of the spherical sediment particle accumulation body was 36.41–43.11%, wherein 26.32% of the pore volume in the accumulation body could be used for gas storage through gas-driven brine drainage [28]. Zheng et al. studied the space utilization possibility of insoluble substance. They measured that the porosity of the laboratory sediments was at least 42.8–50.2%, while gas displacement increased the usable volume by 1.4–2.3% in the experiment [29]. The current research has mostly focused on the morphology and physical properties of sediments, along with the feasibility of the utilization of sediment pore space for gas storage. The understanding of liquid–solid two-phase flow in gas-driven brine drainage in the sediments of salt caverns is the basis of utilizing the sediments pores for gas storage [30,31]. Therefore, the purpose of this paper is mainly to carry out a laboratory simulation experiment of gas-driven brine drainage, and then analyze the flow law of brine and sediment particles, along with its influencing factors.

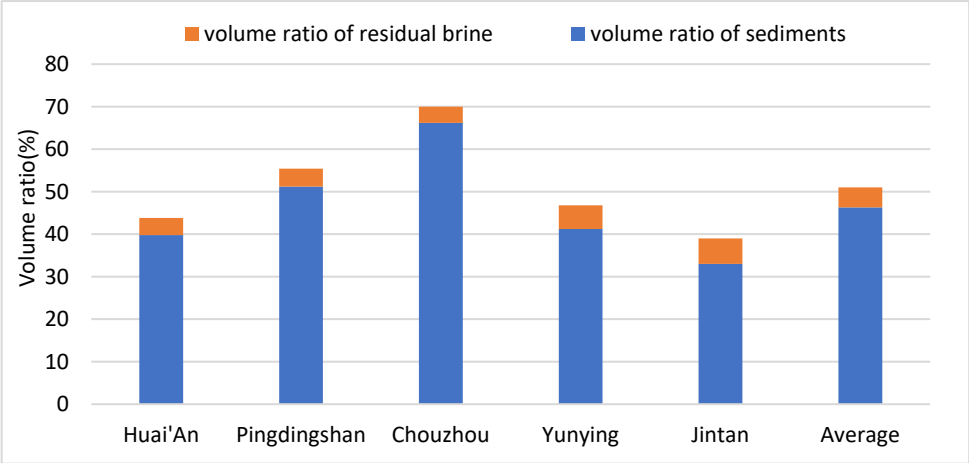

Figure 1. The salt cavern volume occupied by sediment and residual brine in some areas.

2. Test and Analysis of Physical Properties of the Sediments

The salt cavities built and put into operation in China are concentrated in the Jintan District. In order to better integrate the laboratory simulation experiments with the field, insoluble sediments were extracted from the core samples of some salt layers in the Jintan District.

2.1. Preparation of Sediment Samples for Laboratory Experiments

The salt core columns of six salt cavities from the Jintan District were selected to conduct a water solution experiment. The experimental steps were as follows [32–35]:

(i) Identify core columns, weigh and measure them, and record the weight and volume of each core column.
(ii) Place the core samples in different containers in sequence.
(iii) Prepare clean water. The amount of water required for each core column dissolution test is based on its own weight in a ratio of 3 g of salt rock to 10 g of water.
(iv) Pour the water into the corresponding container and soak the core column samples for more than 5 days to completely dissolve the soluble salts in the samples. The clay

and other insoluble materials in the samples will be broken by brine immersion and expansion, and precipitate at the bottom of the container.

(v) Collect the residual sediments of the core columns in all containers; then, dry, weigh and measure them, make a record, and mark them separately.

Table 1 shows the experimental test data of the core columns and their insoluble sediments. Figure 2 shows the labeled sediment samples of the salt core columns from the Jintan District after the water dissolution experiments. The test results show that the content of the insoluble matter in salt rocks of the Jintan District was about 14~21%, which is in agreement with the calculation results of sonar measurements data of 23 salt cavern gas storage wells in this area (Figure 3). Therefore, these sediment samples are representative and can be used as experimental samples.

Table 1. The mass, volume, and proportion of insoluble sediment in salt rock samples.

Sample Number	Core Column Weight, g	Core Column Volume, cm^3	Weight of Insoluble Matter, g	Volume of Insoluble Matter, cm^3	Proportion of Insoluble Matter by Weight, %	Volume Fraction of Insoluble Matter, %
1#	1585.2	727.1	225.1	82.7	14.2	11.4
2#	1469.4	598.9	233.6	92.8	15.9	15.5
3#	1585.2	727.1	272.7	100.1	17.2	13.8
5#	5117.1	2041	992.7	291.6	19.4	14.3
6#	4523	1805	755.3	309.7	16.7	17.2
7#	4066	1256	866.1	267.8	21.3	21.3

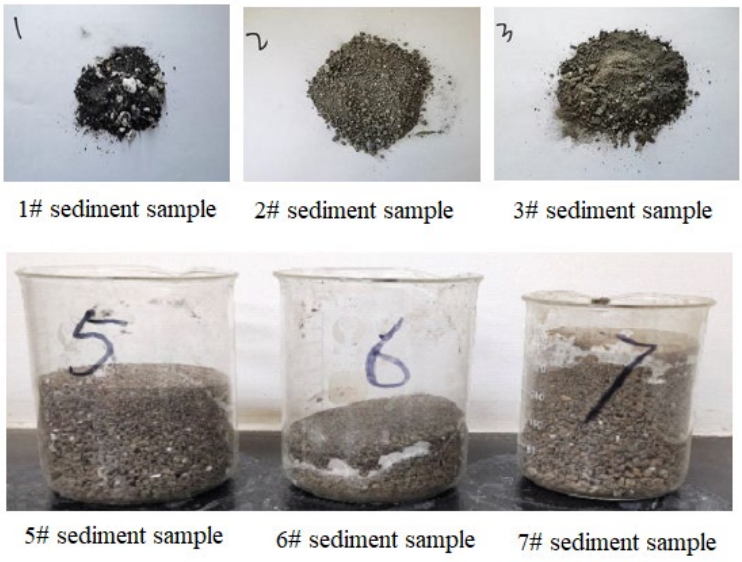

Figure 2. Sediment samples of the salt core columns from the Jintan District after the water dissolution experiments.

2.2. Analysis of Mineral Composition of Insoluble Sediment

The mineral composition of insoluble residue was analyzed by whole-rock X-ray diffraction (XRD), including a whole-rock mineral test and clay mineral test [32–34]. The test results are shown in Tables 2 and 3, and Figure 4.

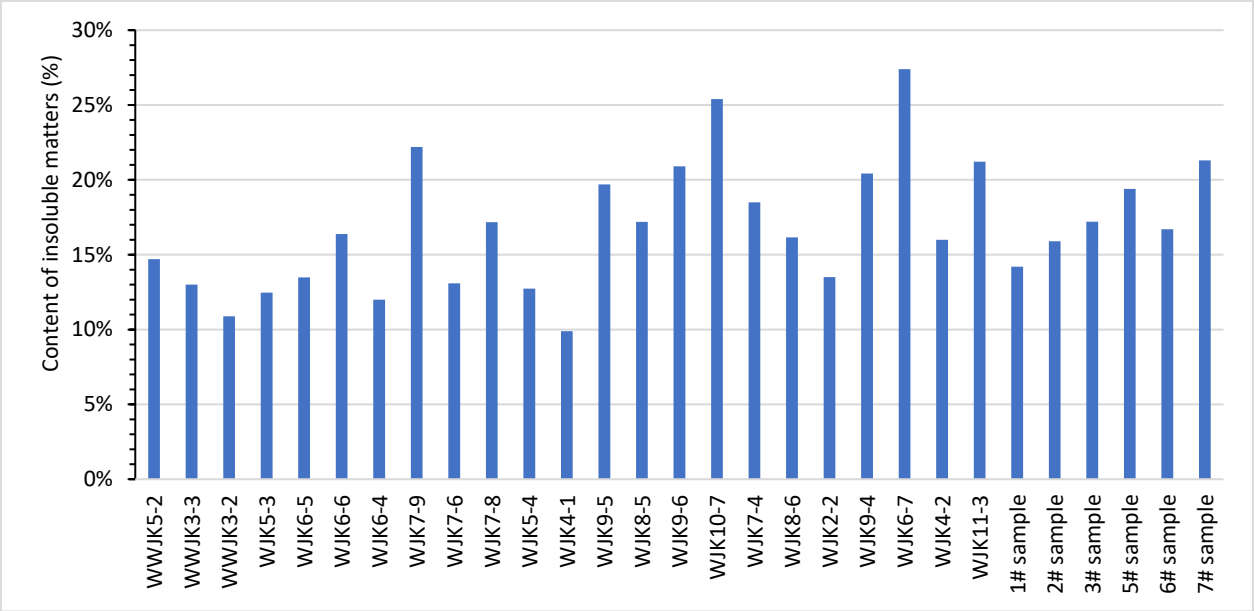

Figure 3. Distribution of the content of insoluble matters in salt rocks of the Jintan District. Note: The data other than the core sample test results are derived from the calculation results of sonar cavity data of salt cavern gas storage wells in Jintan District.

Table 2. Test results of the major mineral compositions and their proportions of the sediments.

Samples	Mineral Composition and Its Proportion (%)									
	Qtz	Kfs	PI	Cal	Dol	Brt	Anh	Gbs	Ank	Clay Mineral
1#	73.7	2.3	20.7	0	0	0	0	0	0	3.3
2#	60.0	4.0	17.6	9.9	0	0	1.8	0	0	6.7
3#	67.6	4.4	14.8	4.6	0	0	3.4	0	0	5.2
5#	28.2	0	6.3	0	0	6.6	0	0.8	43.7	14.4
6#	9.6	1.4	2.6	0	36.6	5.6	0	0	33.1	11.1
7#	57.7	4.7	13.1	0	0	0	1.9	0	18.9	3.7

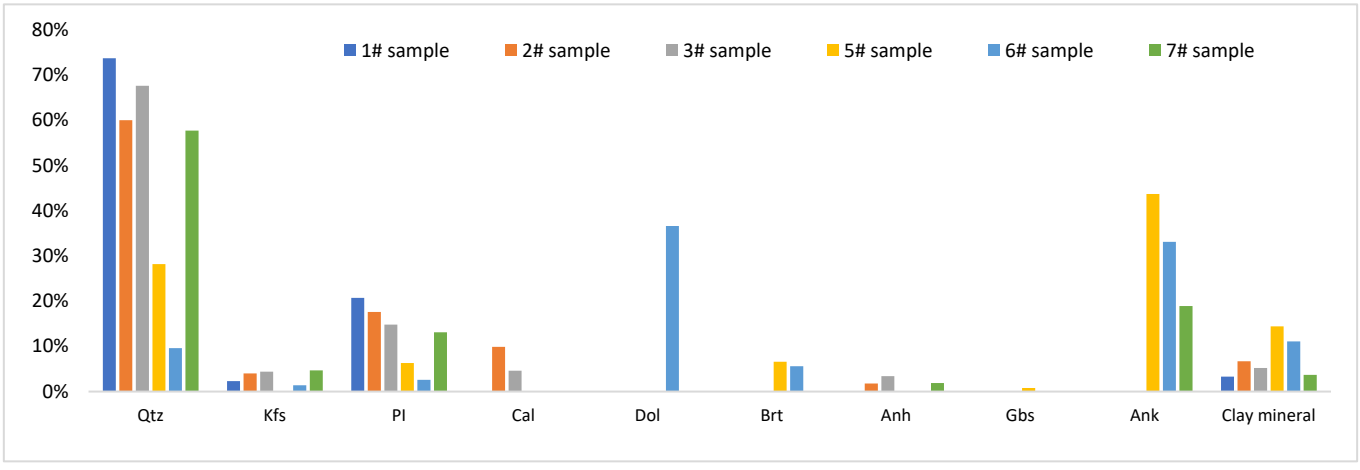

Figure 4. Diagram of the major mineral compositions and their proportions of the sediment. Note: Qtz is quartz, Kfs is potash-feldspar, Pl is plagioclase, Cal is calcite, Dol is dolomite, Brt is barite, Anh is anhydrite, Gbs is gibbsite, and AnK is ankerite.

Table 3. Test results of the main compositions of the clay minerals.

Number of Tests	Relative Content of Clay Minerals (%)		
	I/S	It	C
No. 1	63	32	5
No. 2	51	29	20
No. 3	0	87	13
No. 4	0	74	26
No. 5	0	100	0
No. 6	0	100	0
No. 7	0	100	0
No. 8	0	79	21
No. 9	0	100	0
No. 10	0	100	0
No. 11	10	83	7
No. 12	6	76	18
No. 13	15	81	4
Average	11.1	80.1	8.8

Note: I/S is the mixture of montmorillonite and illite, It is illite, and C is chlorite.

As can be seen from Table 2 and Figure 4, there were more than 10 kinds of mineral compositions in the sediments, of which quartz, plagioclase, and ankerite were the main mineral compositions, accounting for 45–94%, with an average of about 78%. The content of clay minerals in the sediments was about 3.3–14.4%. Illite was the main clay mineral, accounting for about 80.1% of all clay minerals, while others were composed of a mixture of montmorillonite or illite (19.9% on average), as shown in Table 3.

2.3. Particle Size Analysis of Insoluble Sediment

The sieving method was used to determine the particle size distribution of the sediments [36,37]. The experimental steps were as follows:

(i) Prepare sediment samples, and then weigh, mark, and record them;
(ii) Select the proper screens with different mesh numbers according to the design requirements, and stack them in order according to their pore sizes;
(iii) Pour the sediment samples on the highest screen;
(iv) Turn on the vibrating screen machine and use the vibration of the machine to sift the sediments through the installed screens;
(v) Take out the screens of each layer in turn; then, collect the sediment particles on the screen, weigh them, and record the results;
(vi) Calculate and analyze the distribution of different particle sizes of the sediments according to the recorded data.

The tests results are shown in Table 4 and Figure 5.

As can be seen from Table 4 and Figure 5, the particle size distribution of the sediments ranged from 0.04 mm to 6 mm, and the corresponding mesh number ranged from 4 mesh to 360 mesh. The particle size distribution could be divided into four ranges: <0.5 mm, 0.5 mm~2 mm, 2 mm~4 mm and >4 mm. The mass percentage of each range was 37.9%, 36.5%, 17%, and 8.6%, respectively.

Table 4. Test results of the particle size distribution of the sediments.

Seive Mesh (Mesh)	Particle Diameter (mm)	Test 1#	Test 2#	Test 3#	Test 4#	Test 5#	Test 6#
4	6	15.40%	0.16%	1.08%	3.86%	5.56%	5.64%
5	5	7.24%	1.47%	3.23%	2.90%	2.25%	2.58%
6	4	0.47%	0.94%	1.08%	12.02%	10.64%	13.97%
7	3.5	6.13%	5.40%	8.12%	7.60%	6.00%	6.28%
8	3	2.92%	3.93%	2.86%	4.89%	3.77%	5.36%
10	2	2.34%	5.17%	2.98%	18.96%	12.33%	15.98%
12	1.6	3.21%	8.74%	5.90%	10.87%	9.61%	9.42%
16	1.25	5.49%	9.89%	8.62%	13.56%	12.09%	10.53%
20	1	6.41%	12.94%	10.41%	7.73%	8.53%	7.12%
40	0.45	24.83%	26.52%	32.97%	8.52%	10.03%	7.44%
50	0.36	2.72%	2.22%	1.61%	4.70%	4.75%	5.20%
80	0.2	10.01%	9.89%	10.97%	3.20%	6.46%	4.70%
120	0.12	3.88%	4.04%	3.09%	0.99%	3.21%	3.75%
200	0.07	5.57%	5.62%	5.13%	0.13%	4.19%	1.10%
300	0.05	1.97%	1.86%	1.36%	0.04%	0.48%	0.64%
>300	<0.05	1.41%	1.21%	0.59%	0.03%	0.10%	0.29%

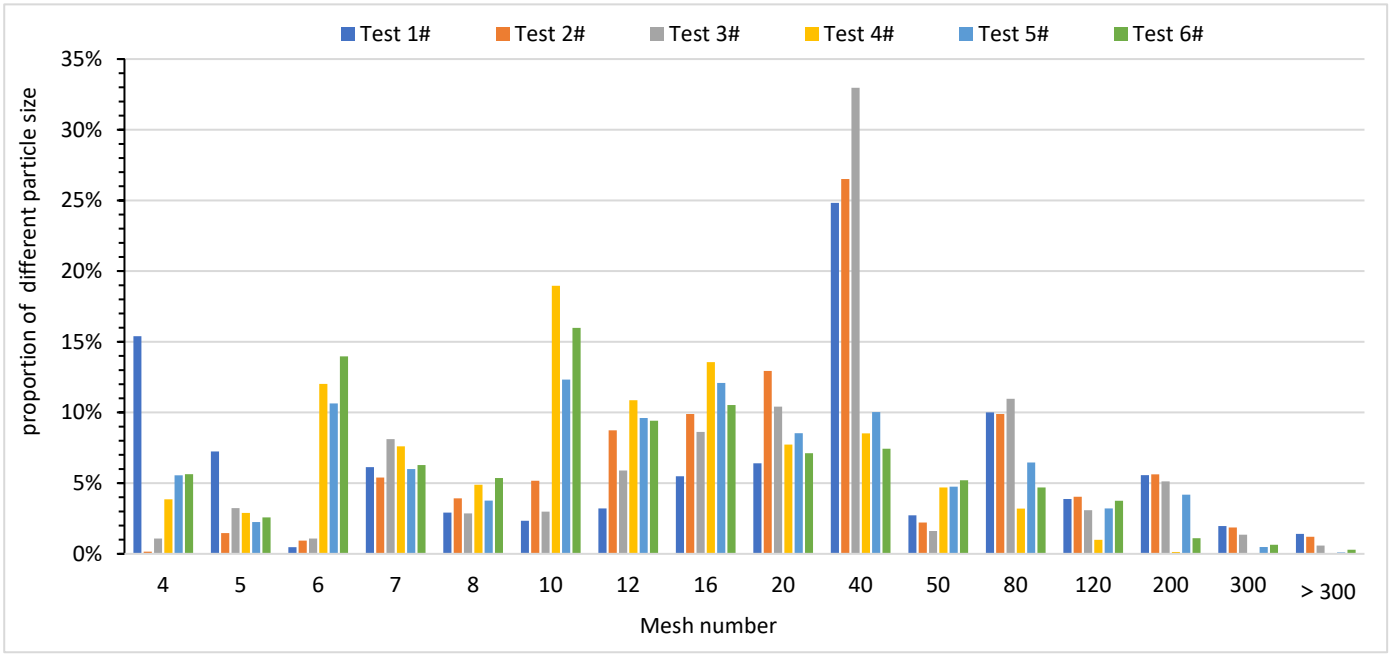

Figure 5. Particle size distribution of sediments.

3. Experimental Methods and Results Analysis

A laboratory simulation device and experimental method of the gas-driven brine drainage were self-designed to analyze the flow law of the brine and sediment particles in gas-driven brine drainage in the sediments of salt cavern gas storage. Using artificial composite sediments in the experimental device, we tested the flow rates of brine and solid particles in the vicinity of the brine drain pipe in the sediments under different nitrogen

displacement pressures, the effect of nitrogen displacement pressure, brine drain time, and brine flow rate on the sand extraction amount.

3.1. The Simulation Experimental Device

In order to facilitate the research and the establishment of experimental equipment, a cylinder was used to simulate the salt cavern without considering the irregular shape of the salt cavern. It was a transparent acrylic cylinder with a diameter of 60 cm and a height of 90 cm, which could achieve the sealing of the simulated salt cavern through a thread connection with the seal cover. There were three sealing connectors on the seal cover, one for connecting the gas injection line, one for installing the simulated brine drainage pipe, and the other for standby. A nitrogen cylinder was connected to the other end of the gas injection line, and a valve was installed near the connection to control the gas displacement. A transparent PE pipe with an outer diameter of 8 mm and an inner diameter of 6 mm was used to simulate the brine drain pipe, of which the bottom end was inserted in the sediments in the simulated cavity, and the top end was connected with the drain line through the sealing connector. Several measuring cups were used to collect and measure the brine discharged through the line. Compared with the salt cavern gas storage in the Jintan District, the simulated salt cavern and the simulated brine drainage pipe were reduced as a whole in a ratio of 1:278.

A schematic diagram of the laboratory simulation experiment device is shown in Figure 6, and a physical diagram is shown in Figure 7.

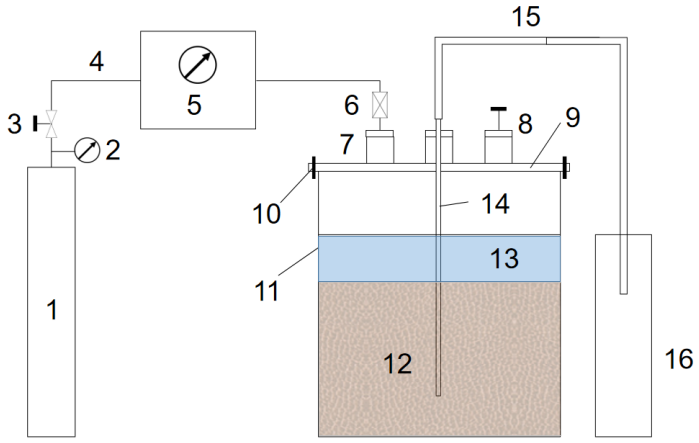

Figure 6. Schematic diagram of the laboratory simulation experiment device. Note: 1. nitrogen cylinder, 2. pressure gauge, 3. valve, 4. gas injection line, 5. pressure gauge, 6. valve, 7. sealing connector, 8. spare connector, 9. seal cover, 10. bolt, 11. simulated salt cavern, 12. sediments, 13. saturated brine, 14. simulated brine drainage pipe, 15. drain line, 16. measuring cup.

Figure 7. The laboratory simulation experiment device in use.

A large number of sediment samples were needed in the laboratory simulation experiments of gas-driven brine drainage, and the sediment samples obtained by dissolving the cores were far from sufficientl therefore, some sediment samples were prepared artificially according to the test results of the physical properties of the sediment.

On the basis of a comparison of the data presented in Tables 5 and 6, the physical parameters of the artificial sediment samples, such as mineral composition and its proportions, and porosity, were slightly different from but generally similar to the actual sediment samples. Therefore, the artificial sediment samples could be used in laboratory experiments and would not bring too much influence on the simulation experiments of gas-driven brine drainage and the study of the flow law of brine and sediment particles in the process of the experiments.

Table 5. Comparison of mineral compositions between artificial sediment samples and real sediment samples.

Sample Number	Mineral Composition and Its Proportions (%)									
	Qtz	Kfs	Pl	Cal	Dol	Brt	Anh	Gbs	Ank	Clay Mineral
Sediment sample 5#	28.2		6.3			6.6		0.8	43.7	14.4
Sediment sample 6#	9.6	1.4	2.6		36.6	5.6			33.1	11.1
Artificial sediment sample 1#	16.9		3.3	9.1	19.0	11.5		1.5	8.7	12.1
Artificial sediment sample 2#	21.2		4.1			5.4	3.5		50.8	13.6
Artificial sediment sample 3#	13.2		2.7		30.6	7.3			27.7	10.0

Table 6. Comparison of porosities between artificial sediment samples and real sediment samples.

Data Sources	Sediment Porosity (%)
Test results of sediment sample 5#	48.34–50.62
Test results of sediment sample 6#	46.48–48.73
Test results of artificial sediment sample 1#	41.36–45.57
Test results of artificial sediment sample 2#	48.92–50.19
Test results of artificial sediment sample 3#	45.27–47.55
Results of numerical model analysis (Han, J. [28])	36.41–43.11
Experimental test results (Zheng, Y. [29])	42.8–50.2
Results of modeling analysis (Ren, Z. [30])	45.9–46.95
Results of sonar cavity measurement (Field data [31])	42.66

3.2. Experimental Conditions and Procedures

The pre-experiment preparation and experimental conditions were as follows:

- The artificial sediment samples were poured into the simulated salt cavern, whose filling height was set at 50 cm~60 cm.
- The brine used in the experiments was taken from the salt cavern gas storage wells in the Jintan District, and it could also be self-configured in accordance with the concentration of 25–26%. After the brine filled the pores of the sediments, the liquid level was kept 10 cm above the sediment surface.
- Three types of simulated brine drainage pipes were prepared; the lower part of the pipes was pre-arranged with 5 mm, 1.5 mm, and 0.5 mm sieve holes. When tested with a simulated brine drainage pipe, it was inserted into the sediments at a depth of about 10 cm from the bottom of the simulated salt cavern.
- The simulated salt cavern was kept sealed during the experiment.
- The experimental temperature was normal, and the experimental pressure was set up in groups (0.005 MPa, 0.01 MPa, 0.015 MPa, 0.02 MPa, 0.025 MPa, 0.03 MPa, 0.035 MPa,

0.04 MPa, 0.045 MPa, 0.05 MPa, 0.1 MPa, 0.15 MPa and 0.2 MPa), controlled by the nitrogen cylinder and valves.

- The experiment consisted of the following steps:
  - (i) Prepare sediments and brine according to the requirement of the experiment condition, and install the experimental equipment to check the air tightness of the simulated salt cavern and the gas injection line;
  - (ii) Pour the sediments and brine into the simulated salt cavern; then, install the simulated brine drainage pipe, and connect the simulated salt cavern and its seal cover by bolts;
  - (iii) Connect the gas injection line to the left sealing joint of the sealing cover, and check the sealing of the simulated salt cavern and the gas injection line again to ensure that no leakage occurs during the experiment;
  - (iv) Connect the drain line with the simulated brine drainage pipe through the middle sealing joint of the sealing cover, and then get the measuring cups and a timer ready;
  - (v) Then, start the gas-driven brine drainage simulation experiments. The flow law of brine and sediment particles near the brine drainage pipe under different pressure is tested by controlling the nitrogen displacement pressure through the valve installed on the gas injection line; meanwhile, the discharge of brine and sediment particles under different pressures and different time are tested. The brine drain time is measured by the timer and the amount of brine discharged is measured by the measuring cups. The amount of sand extracted is determined by collecting and drying the sediment particles in the measuring cups, and then weighing them.
  - (vi) Finally, replace the simulated brine drainage pipe, repeat the previous experiment process, and test the influence of the hole size of the screen on the flow rate of the brine and sediment particles in the sediments, as well as the size and extraction amount of the sediments discharged from the brine drainage pipe.

3.3. Analysis of Experimental Results

3.3.1. The Flow Rate of Brine and Sediment Particles near the Brine Drain Pipe in the Sediments

With parameters such as nitrogen displacement pressure, brine drain time, sand extraction amount, and the reduction ratio of the experimental equipment, the flow rate of brine and sediment particles near the brine drain pipe in the sediments under different injection pressures could be obtained. The relationship between the flow rates of brine and sediment particles and nitrogen displacement pressure is shown in Figure 8.

It can be seen in Figure 8 that the variation of brine flow rate with nitrogen displacement pressure near three kinds of brine drainage pipes was generally similar. There was a threshold pressure of starting flow for the gas-driven brine drainage in sediments due to the flow resistance, where the larger the diameter of the sieve hole, the smaller the threshold pressure. Once the nitrogen displacement pressure exceeded the pressure threshold, the flow rate of brine increased with the increase in nitrogen displacement pressure. Furthermore, the diameter of the sieve hole had a differential influence on the flow rate of the sediment particles near the brine drain pipe. For the brine drain pipes with 1.5 mm diameter sieve holes and 0.5 mm diameter sieve holes, when the nitrogen displacement pressure reached the threshold pressure and the brine began to flow, the flow rate of the sediment particles near the brine drainage pipe was maximum, and then decreased rapidly with the increase in nitrogen displacement pressure, before gradually becoming stable. However, for the brine drain pipe with 5 mm diameter sieve holes, the flow rate of the sediment particles near the brine drainage pipe firstly reached a higher value as the brine began to flow, and then decreased rapidly, before increasing gradually with the increase in nitrogen displacement pressure in a fluctuating manner.

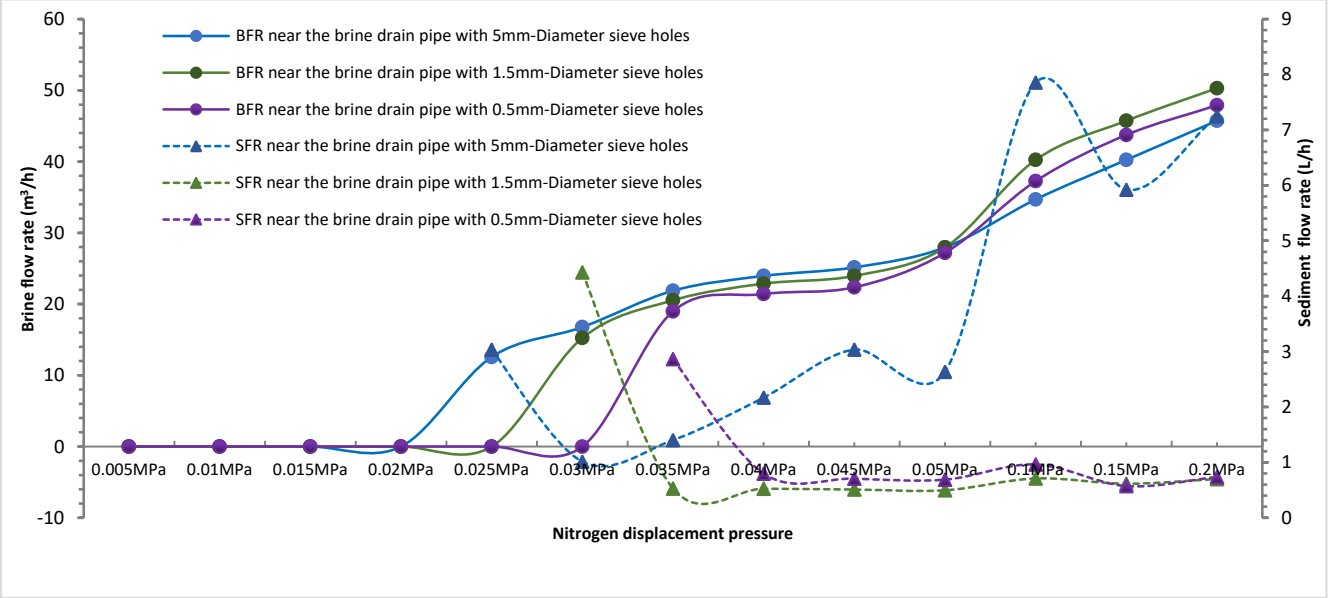

Figure 8. Relationships of brine flow rate (BFR) and sediment flow rate (SFL) with the increase in nitrogen displacement pressure in the vicinity of brine drain pipe with different sieve holes.

3.3.2. Effect of Nitrogen Displacement Pressure on Sand Extraction Amount

During the experiments of gas-driven brine drainage, the change in nitrogen displacement pressure affected the brine flow rate, which affected the extraction amount of sediment particles. Figure 9 shows the sand extraction amounts of three kinds of brine drain pipes with different diameters of sieve holes under different nitrogen displacement pressures. It can be seen from the diagram that a larger diameter of the sieve hole facilitated sanding of the pipe. The sand extraction amounts of these three pipes were basically the same with the change in nitrogen displacement pressure; that is, the initial sand extraction amount was generally high, and then it fluctuated with the increase in nitrogen displacement pressure, showing a positive correlation in general.

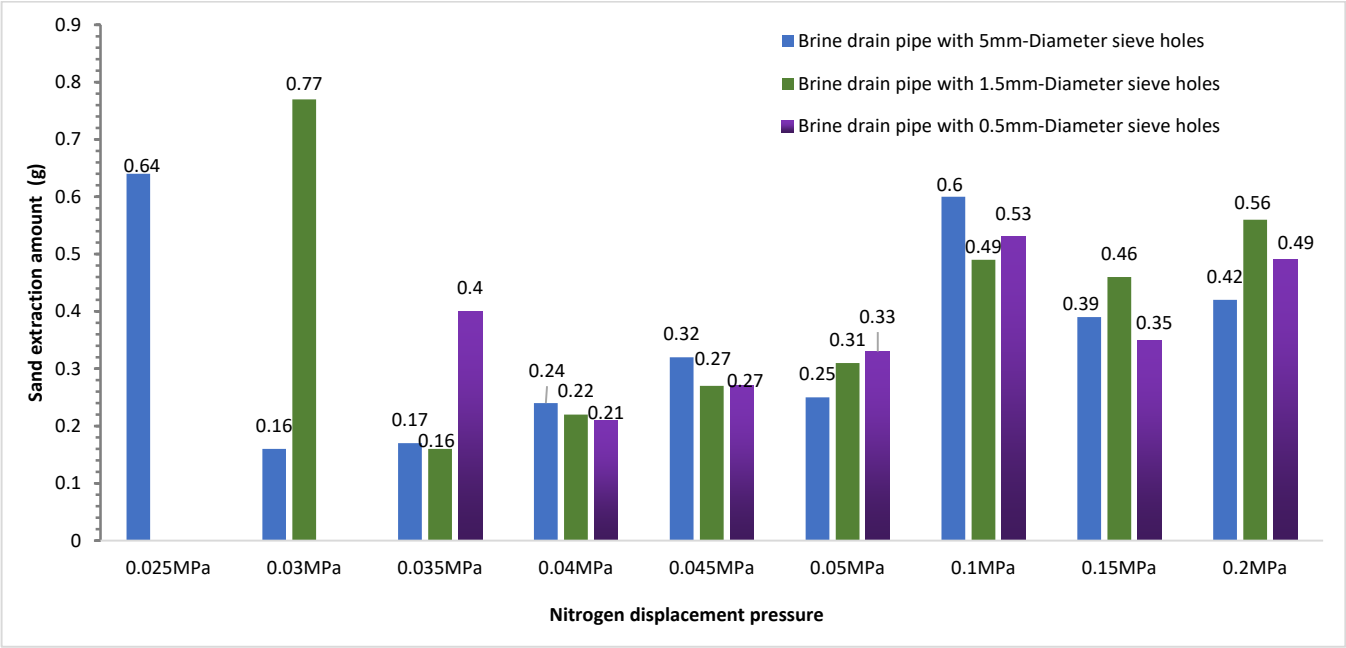

Figure 9. Relationship between sand extraction amount and nitrogen displacement pressure of different brine drain pipes.

3.3.3. Effect of Brine Drain Time on Sand Extraction Amount

In this experiment, we tested the relationships of sand extraction amount of different sizes of sediment particles and cumulative amount of sediment particles with brine drain time. The test results are as shown in Figures 10 and 11.

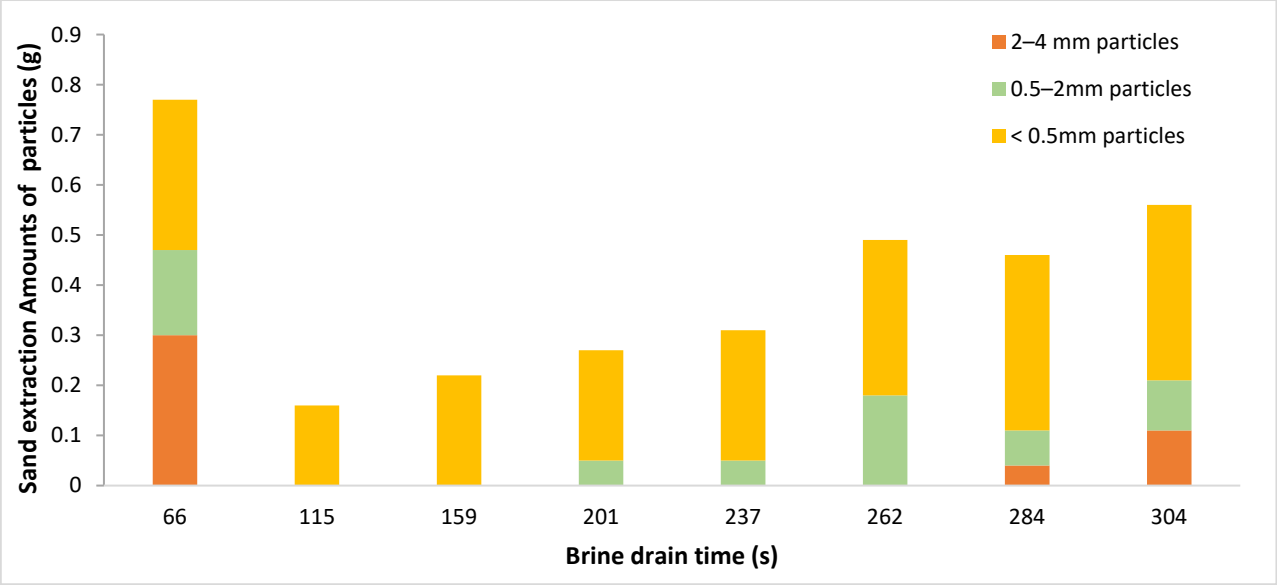

Figure 10. Relationship of the amounts of different sizes of sediment particles with the brine drain time (brine drain pipe with 1.5 mm diameter sieve holes).

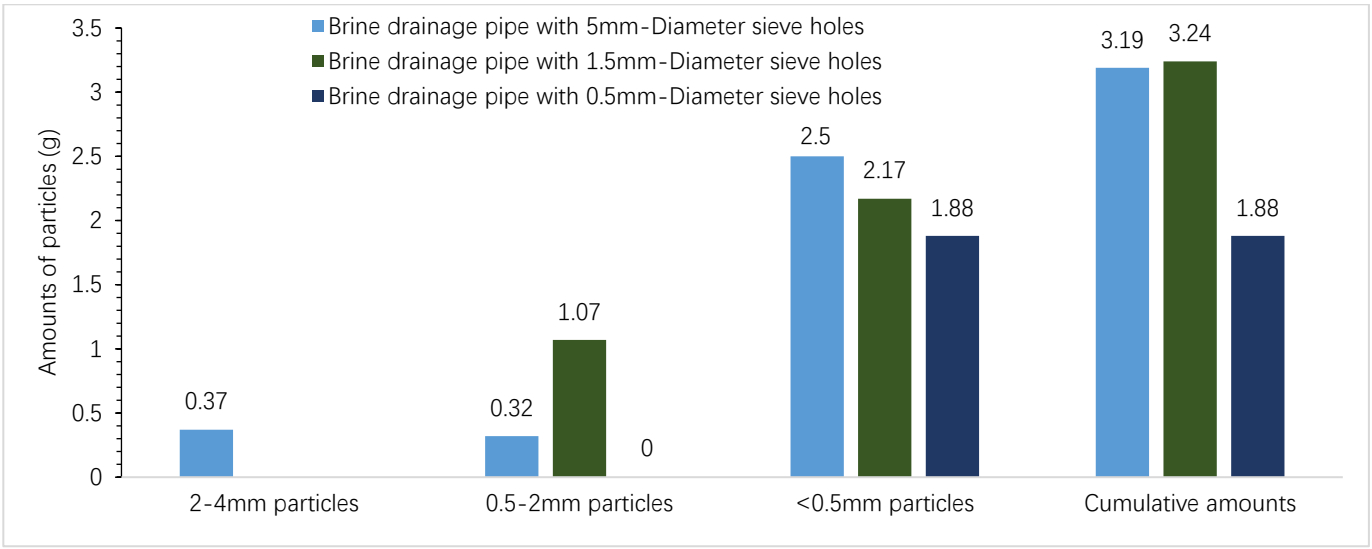

Figure 11. Comparison of the amounts of sediment particles discharged with brine in three kinds of brine drainage pipes.

It can be seen in Figure 10 that, at the early stage of the experiment, a large number of different sizes of sediment particles less than 4 mm in diameter were discharged with brine; the sand extraction amounts of sediment particles with diameters of 2–4 mm, 0.5–2 mm, and less than 0.5 mm were 0.3 g, 0.17 g, and 0.3 g, respectively. Subsequently, the sand extraction amounts decreased rapidly, and only sediment particles less than 0.5 mm in diameter were discharged. With the increase in brine drain time, the sand extraction amounts of particles less than 0.5 mm in diameter gradually increased, and the particles

with diameter of 0.5–2 mm and 2–4 mm were also discharged gradually; the total sand extraction amount showed a positive correlation with the brine drain time.

The reason for this trend may have been related to the distribution of sediment particle size and the diameter of sieve hole. According to the previous experimental results, 91.4% of the sediment particles were less than 4 mm in diameter; therefore, most of the sediment particles near the brine drainage pipe could enter the pipe through the 5 mm diameter sieve holes and be discharged with the brine, and the initial sand extraction amounts of sediment particles were relatively high. However, when a large number of particles with larger size moved to the vicinity of the brine drainage pipe, some of them could come into contact with each other to form a "sand bridge" near the sieve holes. This played a certain role of "sand control" on the pipe and only allowed the fine-sized sediment particles to pass through with the brine. Meanwhile, there was flow resistance on the particles in the surrounding sediments moving toward the pipe. As a result, the sand extraction amounts decreased rapidly, and only some sediment particles less than 0.5 mm in diameter were discharged. Subsequently, with the increase in brine drain time, the peripheral sediment particles continuously moved to the vicinity of the pipe along with the brine, and the sand extraction amount gradually increased. The stability of the sand bridge structure near the pipe could be destroyed when the nitrogen displacement pressure fluctuated or the brine flow rate increased suddenly, whereby the sediment particles with diameter of 0.5–2 mm were gradually discharged with the brine through the sieve holes, and different sizes of particles near the pipe were carried out with the brine through the pipe again.

Figure 11 shows the amount and comparison of various kinds of sediment particles discharged with brine in three kinds of brine drainage pipes during the experiment. As can be seen from the Figure 11, the particles less than 0.5 mm in diameter constituted the main parts of the sediments that were discharged, accounting for 100%, 67%, and 78% of the sediments discharged with brine in the three kinds of pipes. The diameter of the sieve hole had a certain impact on the cumulative sand extraction. The cumulative amounts of particles discharged from the pipes with 5 mm diameter and 1.5 mm diameter sieve holes were almost the same, being about 1.7 times that discharged from the pipe with 0.5 mm diameter sieve holes.

Therefore, in order to prevent too many sediment particles from entering the brine drainage pipe and causing blockage or erosion of the pipe, two suggestions are put forward when the operation of gas-driven brine drainage in the sediments is carried out on the spot: (i) a screen pipe with 1 mm diameter sieve holes is suggested to be used for sand control; (ii) sieve holes are recommended to be machined in the shape of a trumpet with a small inlet section (i.e., 1 mm) and a large outlet end (i.e., 1.5 mm). The significance of this is that the sediment particles do not easily bridge each other and plug the sieve hole upon passing through the screen pipe. Even if they are blocked, this is also conducive to the removal of pipe plugs using the positive cycle cleaning method.

3.3.4. Effect of Brine Flow Rate on the Sand Extraction Rate

The sand extraction rate at different brine flow rates was tested and analyzed, and the results are shown in Figure 12. It can be seen in Figure 12 that the sand extraction rate increased with the increase in brine flow rate. When the brine flow rate was between 20 m^3/h and 30 m^3/h, the sand extraction rate of the brine drainage pipe was relatively low, at only about 0.2–0.3 g per liter. However, the sand extraction rate doubled to 0.4–0.5 g per liter when the brine flow rate reached 35–50 m^3/h. The reason for the higher initial sand extraction rate is that a large number of sediment particles with diameter less than 0.5 mm near the brine drain pipe were discharged with the brine when the brine began to flow. This speed was instantaneous, and its duration was not long. According to the experimental results, taking into account the factors such as sand production rate and the minimum discharge requirements for the pipe string to carry sediments, the brine flow rate is suggested to be about 30 m^3/h, depending on the actual operation on site.

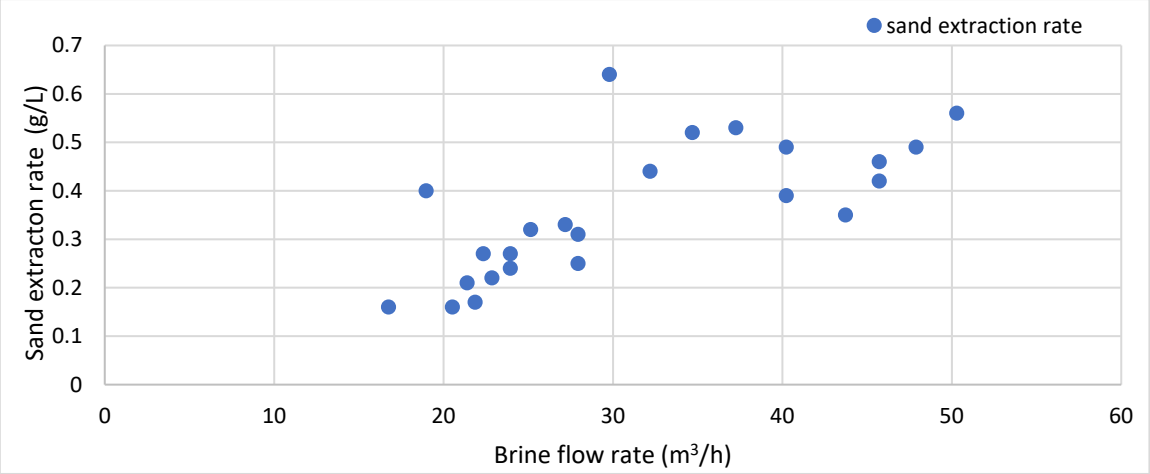

Figure 12. The relationship between the sand extraction rate and the brine flow rate.

4. Conclusions and Discussion

In this paper, the physical properties of insoluble sediments of salt rocks from the Jintan District were tested, a self-designed laboratory experimental apparatus and method for simulating gas-driven brine drainage in sediments were introduced, and the flow law of brine and sediment particles in the simulated experiments was tested. The main conclusions are as follows:

1. Quartz and dolomite are the main mineral components of the insoluble sediments from salt rocks in the Jintan District, accounting for 45–79%, and the clay mineral content is about 5–15%.
2. There is a threshold pressure for the gas-driven brine drainage in the sediments. A larger diameter of the sieve hole results in a smaller threshold pressure. Once the nitrogen displacement pressure exceeds the threshold pressure, the flow rate of brine and sand extraction amount increases with the increase in nitrogen displacement pressure.
3. The diameter of the sieve hole has an effect on the liquid–solid two-phase flow in the sediments near the brine drain pipe, as well as a greater effect on the flow rate of the sediment particles. The screen pipe with 1 mm diameter sieve holes is suggested to be used for sand control, and the sieve holes are recommended to be machined in the shape of a trumpet with a small inlet section (i.e., 1 mm) and a large outlet end (i.e., 1.5 mm) when the operation of gas-driven brine drainage in the sediments is carried out on the spot.
4. The sand extraction amount is influenced by many factors in the process of gas-driven brine drainage, such as the nitrogen displacement pressure, the diameter of the sieve hole, the brine drain time, and the brine flow rate. A higher nitrogen displacement pressure and brine flow rate result in more sand extraction. According to the experiment results, the brine flow rate is suggested to be about 30 m^3/h when the brine removal is carried out in the sediments of salt cavern, but this depends on the actual operation on site.
5. The salt caverns for gas storage are mainly built in salt beds with many inter-layers in China, and over one-third of the volume of the salt cavern is occupied by insoluble sediments. Extensive research results show that these sediments in the salt cavern have large pore space and good potential for gas storage. It is estimated that, if 20% brine can be discharged from the sediments of a salt cavern, the gas storage volume can be increased by 17.6%. The experimental equipment and method presented in this paper can be used to simulate the gas-driven brine drainage experiment in the laboratory. The research on the flow law of brine and sediment particles in the sediments has certain reference and guiding significance for the field operation of gas-driven brine drainage and expansion of gas storage capacity in the salt cavern.

6. There are still some limitations in these experiments. For example, the sediment samples used were artificially prepared on the basis of the test results of insoluble matters in salt rocks from the Jintan District. There must be a difference between the artificial sediment samples and the actual sediments at the bottom of the salt cavern. In addition, the simulation experiment time was relatively short, and the influence of salt crystallization blocking was not considered in the experiment [38,39]. Therefore, the experimental method needs to be improved continuously, and the laws and cognition need to be further studied.

Author Contributions: Methodology, Y.Z. and E.Y.; validation, J.L. (Jun Li); investigation, J.L. (Jun Lu); data curation, Y.Z. and Y.L.; writing, Y.Z. All authors have read and agreed to the published version of the manuscript.

Funding: This research was financially supported by the fund project of CNPC (2020D-5008-12) and technology development project of CNPC (2022KT2203).

Institutional Review Board Statement: Not applicable.

Informed Consent Statement: Not applicable.

Data Availability Statement: Not applicable.

Conflicts of Interest: The authors declare no conflict of interest.

References

1. Ma, H. A preliminary study on the development current situation of salt cavern gas storage in China. *China Well Salt Rock* **2021**, *52*, 12–15.
2. Wanyan, Q.; An, G.; Li, Z.; Li, D.; Gou, Y.; Ran, L.; Bai, S. Status and development direction of salt-cavern gas storage technologies. *Oil Drill. Prod. Process.* **2020**, *42*, 444–448.
3. Yang, H. Construction key technologies and challenges of salt-cavern gas storage in China. *Oil Gas Storage Transp.* **2017**, *36*, 747–753.
4. Ran, L.; Guo, K.; Wang, L. Current status and future development trend of underground gas storage in the world. In Proceedings of the First International Conference on Technological Innovation and Intelligent Development of Underground Storage, Langfang, China, 14 October 2016; pp. 233–238.
5. Zhang, B.; Lv, B.; Wu, Y.; Cui, L.; Zhou, S. Development and Trend of Salt-Cavern Gas Storage in Domestic and Abroad. *China Well Salt Rock* **2021**, *52*, 21–24.
6. Xue, Q.; Luo, L.; Zhang, Z. Considerations and suggestions on the construction of salt cavern gas storage in China. *Sci. Manag.* **2019**, *21*, 93–95.
7. Ding, G.; Li, C.; Wang, J.; Xu, H.; Zheng, Y.; Wanyan, Q.; Zhao, Y. The status quo and technical development direction of underground gas storages in China. *Nat. Gas Ind.* **2015**, *5*, 107–112. [CrossRef]
8. Jiang, D.; Ren, T.; Chen, J.; Ren, S.; Fan, X.; Yang, C. Experimental study on mechanical properties of salt rock with weak intercalation. *J. Rock Mech. Eng.* **2012**, *9*, 1797–1803.
9. Dai, X.; Zhang, G.; Tang, L.; Ma, J. Causes Analysis and Solutions of JT2 Well Blocking in Jintan Salt-cavern Gas Storage. *China Well Rock Salt* **2017**, *1*, 13–15.
10. Li, J.; Ba, J.; Liu, C.; He, B.; Li, S.; Chen, J. Problems in the field of Jintan Salt-Cavern Gas Storage and their countermeasures. *Oil Gas Storage Transp.* **2017**, *36*, 982–986.
11. Liu, C.; Xu, L.; Xian, X. Kinetics characteristics of resolving of rock salt of Changshan in Dynamic state. *J. Chongqing Univ. (Sci. Technol. Ed.)* **2000**, *4*, 58–71.
12. Zeng, Y.; Chen, M. Experimental determination of salt wellbore dissolution rate. *Pet. Drill. Technol.* **2003**, *3*, 1–3.
13. Zhang, Q.; Liu, D.; Jia, C. Development of similar materials for geomechanical model of salt rock oil and gas storage media. *Geotech. Mech.* **2009**, *12*, 3581–3586.
14. Zheng, Y.L.; Zhao, Y.J.; Ding, G.S. Solution mining technology of enlarging space for thick-sandwich salt cavern storage. *Pet. Explor. Dev.* **2017**, *44*, 137–144. [CrossRef]
15. Zheng, Y.; Zhang, H.; Wang, Z.; Ding, G. Experimental study on mechanical property of rock satl with impurity. *J. China Coal Soc.* **2012**, *1*, 17–20.
16. Liu, W.; Li, Y.P.; Yang, C.H.; Ma, H.J. Investigation on permeable characteristics and tightness evaluation of typical inter-layers of energy storage caverns in bedded salt rock formations. *Chin. J. Rock Mech. Eng.* **2014**, *33*, 500–506.
17. Ban, F.; Gao, S.; Shan, W. Rock salt grades influences on salt cavity gas storage built with water solution. *Nat. Gas Ind.* **2006**, *4*, 115–118.

18. Wang, Y.G.; Chen, J.S.; Liu, C.; Li, J.J. The technology for controlling the collapse of thick interlayer during the construction of salt-cavern gas storage. *Oil Gas Storage Transp.* **2017**, *38*, 1035–1041.
19. Wang, J.; Ba, J.; Wang, W. Distortion influence on cavern volume of Jintan salt cavern gas storage. *J. Southwest Pet. Univ. (Sci. Technol. Ed.)* **2022**, *44*, 105–113.
20. Yuan, C. Theoretical analysis of the inter-layer collapse in solution mining of the salt cavern. *Sci. Technol. Eng.* **2015**, *2*, 14–20.
21. Guo, K.; Li, J.; Zheng, X. Inter-layer treatment process in cavity building for salt cavern gas storage: A case study of Jintan Gas Storage of West-to-East Gas Pipeline. *Oil Gas Storage Transp.* **2015**, *2*, 162–166.
22. Men, J. Development and application of salt cavity gas storage reservoir technology. *J. Gas Heat.* **2019**, *6*, 4–8.
23. Du, Y.; Kang, Y. Discussion and practice on the technology of first gas injection and brine discharge in salt cavern gas storage. *Petrochem. Ind. Appl.* **2019**, *38*, 63–66.
24. Ji, X.; Liu, Y.; Wang, Z.; Zhang, J.; Wang, A.; Ye, W. Study and application of brine discharge and capacity expansion technology for salt cavern gas storage in Jintan District. *Chem. Eng. Equip.* **2020**, *4*, 121–123.
25. Chen, X.; Zhang, L. Experimental study on the coefficient of expansion of sediment in multi-layered salt cavern reservoirs. *Min. Res. Dev.* **2013**, *2*, 34–37.
26. Ren, Z.; Yang, H.; Li, J.; Liu, J.; Fan, Z. Test and calculation of void volume of deposit at the bottom of salt rock storage. *J. Southwest Pet. Univ. (Sci. Technol. Ed.)* **2018**, *40*, 142–150.
27. Zhang, Y.; Lu, J.; Li, J.; Ran, L.; Liu, Y. Mechanism analysis of enlarging the gas storage capacity of the cavity by utilizing void space of the sediments at the bottom of the salt cavern. In Proceedings of the 33rd National Symposium on Natural Gas, Nan-ning, China, 31 May–2 June 2023; pp. 286–292.
28. Han, J. *Study on the Void Volume of Deposits at the Bottom of Salt Cavern Gas Storage*; Southwest Petroleum University: Chengdu, China, 2015; pp. 52–57.
29. Zheng, Y.; Qiu, X.; Ding, G.; Zhao, Y.; Zhang, M.; Lai, X. Experimental research on using residue void space in salt cavern gas storage. *J. Salt Sci. Chem. Ind.* **2019**, *48*, 14–19, 23.
30. Ren, Z.; Li, J.; Ba, J.; Jiang, H. Expanding capacity of deposits at the bottom of salt rock gas storage chamber and its application. *Nat. Gas Technol. Econ.* **2017**, *11*, 43–45.
31. Li, P.; Li, Y.; Shi, X.; Liang, X. Pore characteristics and volume capacity evaluation of insoluble sediments for gas storage in multi-interbedded salt formations. *Rock Soil Mech.* **2022**, *43*, 76–86.
32. Shi, X.; Li, Y.; Yang, C.; Du, D. Test study of influence of brine on tensile strength of muddy intercalation. *Chin. J. Rock Mech. Eng.* **2009**, *28*, 2301–2308.
33. Sun, C.; Hou, J.; Ding, G.; Wanyan, Q.; Ran, L.; Gou, Y.; Li, K. Study on sedimentation rule of insoluble residual particles in brine of salt cavern gas storage. *J. Salt Sci. Chem. Ind.* **2017**, *46*, 10–12.
34. Ren, Z.; Yang, H.; Li, J.; Ba, J.; Liu, J. Study on the fractal of the void volume of the deposits at the bottom of salt rock gas storage chamber. In Proceedings of the Annual Meeting of Chinese Geo-Science Union, Beijing, China, 15–18 October 2017.
35. Zhang, Y.; Zhang, K.; Li, J.; Luo, Y.; Ran, L.; Sheng, L.; Yao, E. Study on Secondary Brine Drainage and Sand Control Technology of Salt Cavern Gas Storage. *Sustainability* **2023**, *15*, 7793. [CrossRef]
36. Zhang, C. *Study on Density Estimation Method of Graded Particle Bulk*; South China University of Technology: Guangzhou, China, 2013; pp. 79–92.
37. Qin, W.; Sha, A. Fractal characteristics of particle size distribution of silt. *J. Chang. Univ. (Sci. Technol. EC.)* **2009**, *6*, 10–14.
38. Jin, X. *Study on the Rule of Crystal Plugging in Brine Drain Pipe Column of Salt Cavern Gas Storage*; China University of Petroleum: Beijing, China, 2017; pp. 5–21.
39. Jin, X.; Xia, Y.; Yuan, G.; Zhuang, X.; Ban, F.; Dong, A. An experimental study on the influencing factors of salt crystal in brine discharge strings of a salt-cavern underground gas storage (UGS). *Nat. Gas Industry.* **2017**, *4*, 130–134.